LCLS-TN-04-15
UCRL-PROC-207494

X-ray Transport Optics and Diagnostics Commissioning Report

Richard M. Bionta,
Lawrence Livermore National Laboratory.

October 23, 2004

LCLS Diagnostics and Commissioning Workshop,
SLAC, Stanford, CA, September 27-28, 2004

Disclaimer

Auspices

This work was performed under the auspices of the U.S. Department of Energy by University of California, Lawrence Livermore National Laboratory under Contract W-7405-Eng-48.

X-ray Transport Optics and Diagnostics Commissioning Report

Richard M. Bionta, Lawrence Livermore National Laboratory, October 23, 2004

Abstract

We discuss commissioning work funded through LCLS WBS element 1.5: X-ray Transport Optics and Diagnostics (XTOD.) A short description of the XTOD commissioning diagnostics hardware is followed by a brief discussion of FEL induced damage considerations. The remainder discusses simulation work on the response of the Direct Imager camera to a mix of spontaneous and FEL radiation and a Monte Carlo Calculation of the reflections of the spontaneous radiation in the undulator vacuum tube.

XTOD Layout

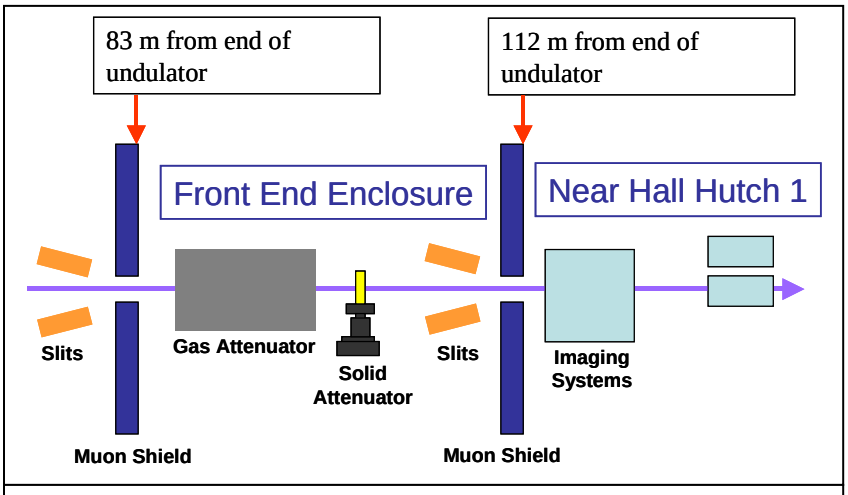

Figure 1: X-Ray instrumentation for commissioning shown schematically through the 1st hutch of the Near Experimental Hall. The Direct Imager and the Indirect Imager are located in the Imaging Systems Tank in the Near Hall Hutch 1.

The XTOD elements relevant to LCLS commissioning are located in the tunnel leading up to the Near Experimental Hall (NEH) and also in the first hutch of the NEH. These are shown schematically in figure 1. The first muon shield defines the boundary between the electron dump area and the "Front End Enclosure" (FEE), which extends to the second muon shield just in front of the NEH. The instrumentation includes a set of horizontal and vertical slits at the beginning and end of the FEE, which the user can use to exclude

the spontaneous halo surrounding the FEL. The gas attenuator in the FEE is a windowless gas chamber that can be used to attenuate the FEL at photon energies below 2 keV. A set of low-z solid attenuators provides attenuation at photon energies above 2 keV. The first hutch in the NEH contains the commissioning diagnostics including a set of imaging cameras for measuring the beam footprint and intensity, and an interchangeable calorimeter or spectrometer.

Dose Considerations

Table 1: Dose to melt and expected dose for selected materials in NEH hutch 1.

		Melt dose	Dose in NEH Hutch 1	
	Z	ev/atom	1 keV	8 keV
Beryllium	4	**0.58**	**0.013**	**0.000**
Diamond	6	**2.13**	**0.062**	**0.002**
Aluminum	13	**0.20**	**0.072**	**0.058**
Silicon	14	**0.91**	**0.100**	**0.078**
Copper	29	**0.44**	**0.183**	**0.142**
Molybdenum	42	**1.24**	**0.993**	**0.649**
Tin	50	**0.14**	**1.873**	**1.292**
Tungsten	74	**1.06**	**1.316**	**1.341**
Lead	82	**0.14**	**2.016**	**2.042**

The post title I positions of the diagnostics are considerably farther from the end of the undulator than originally planned, and as a consequence suffer considerably less dose due to beam divergence especially at lower energies. Table 1 shows the dose suffered by selected materials placed in the peak of the LCLS FEL spatial distribution for 1 bunch for FEL photon energies of 1 keV and 8 keV. These doses should be compared to the dose required to melt the material, given in the third column. The dose is higher at lower photon energies and higher still for high-Z materials. Beryllium, Diamond, and Silicon suffer doses less than a tenth of melt, so will probably survive single shots at full LCLS power. Aluminum and copper are marginal, suffering doses of a third to a half of melt. The higher Z materials are dangerously close to, or well above melt, so will suffer damage on single shots. Nevertheless, is clear that the low Z solids, beryllium, boron carbide, graphite, etc., will not suffer high doses, and can be used as attenuators at all photon energies.

Direct and Indirect Imaging Cameras

The main diagnostics for detecting the FEL in the presence of the spontaneous background are imaging cameras that produce images of the footprint of the LCLS beam at high spatial resolution. The high spatial resolution allows the FEL signal, which is concentrated in a few pixels, to be separated from the spontaneous background, which is spread out over many pixels.

The Direct Imager is a basic camera, shown in figure 2, and utilizes a thin scintillator to convert x-ray photons to visible light. The visible light is collected by a microscope objective and focused on to a CCD camera. This arrangement has many benefits for the LCLS: 1) it separates the x-ray detection from the imaging electronics allowing us to swap in the latest CCD technology; 2) the spatial resolution is determined mostly by the microscope objective, and can be as fine as one micron; and 3) the thin scintillator is not efficient for high energy photons in the spontaneous halo thus reducing background. The main disadvantages are 1) the scintillator is placed directly in the beam and will suffer damage at full FEL power levels unless protected by attenuators; and 2) the sensitivity of this configuration is low due to the small solid angle of the scintillator light captured by the microscope objective.

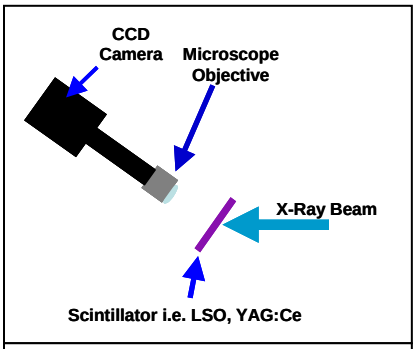

Figure 2: Schematic of the Direct Imager X-Ray camera.

The Indirect Imager is an alternative imaging system that avoids the problem of damage by using a beryllium mirror to reflect a small amount of FEL radiation onto a scintillator. The scintillator/CCD portion of the indirect Imager is the same as the Direct Imager. Calculation show that the mirror need only reflect 0.1 - 1 % of the FEL radiation to provide a good signal in the camera.

Spontaneous Radiation Models

We use the UCLA generated spontaneous radiation data (see the contribution by Sven Reiche “Spontaneous Radiation at the LCLS” in this workshop) to calculate the backgrounds in our instruments. The UCLA data, which consists of 2 GB HDF5 files for each Z along the beam line, is converted to a Paradox database for use on the PC. The spontaneous radiation calculation results in a “cube” of data, two of whose axes give the transverse photon position, and the third axis is photon energy. Each cell of the cube contains the number photons in that spatial and energy bin for 1 LCLS pulse.

Figure 3 shows the near field spatial distributions of the spontaneous radiation for the low linac setting (4.5 GeV) and the high linac setting (14.5 GeV.) Each pixel in the distribution is the energy-weighted sum of all photons striking that pixel. The distributions are narrower in the vertical direction and wider in horizontal direction. The

distribution at the low energies is quite wide, over 10 cm in the horizontal direction. At the highest linac energy the distribution is narrower as expected, and is around 4 cm wide in the horizontal direction. Note that the low energy beam carries 1.85 mJ and the high energy beam carries 18.2 mJ of energy per pulse.

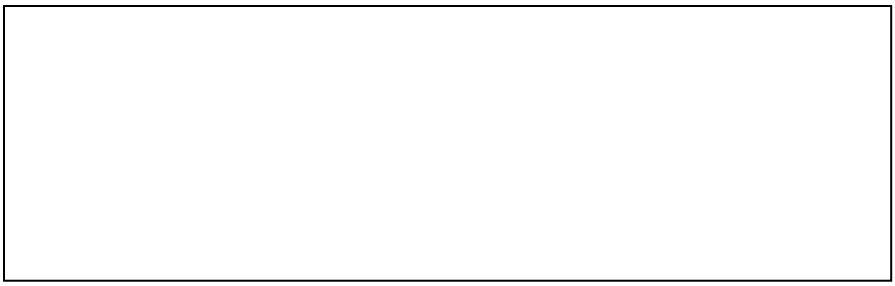

Figure 3: Spontaneous Fluence at the entrance to NEH Hutch 1, 243 m from the beginning of the undulator. The image on the left is for a 4.5 GeV electron beam. The spatial resolution is 1 mm (horizontal) x 300 microns (vertical), and the total energy in the image is 1.85 mJ. The image on the right is for a 14.5 GeV electron beam. The spatial resolution is 300 x 100 microns, and the total energy in the image is 18.2 mJ.

Calculating Direct Imager Signal Levels

To calculate the signal levels in the Direct Imager we start with the cube of spontaneous data and calculate the number photons in each spatial/energy coordinate that are absorbed in 25 μm of LSO scintillator. This results in another cube of data representing the photons absorbed in the scintillator at each position and energy. This cube of absorbed photons is fed into the camera/scintillator simulation, which calculates the number of visible photons emitted by the scintillator and the number that actually strike the CCD pixel. The camera simulation then converts the number photons striking each pixel into the number of photoelectrons generated in each pixel using the quantum efficiency of the CCD and emission spectrum of the scintillator. The number of photoelectrons in each pixel is the relevant figure of merit for the CCD signal and should be compared against the CCD full well and the noise levels due to shot noise, readout noise, and dark current noise.

The camera/scintillator simulation was verified against measurements of a prototype Direct Imager constructed in FY 2002. The prototype imager had a 25 μm thick LSO scintillator viewed by a Zeiss 2.5x microscope objective (NA = 0.12.) The CCD was a backthinned array of 1024 x 1024 square pixels each 24 μm on a side. The measurements were preformed at SPEAR beam line 2-3 x-ray energies between 6 -20 keV.

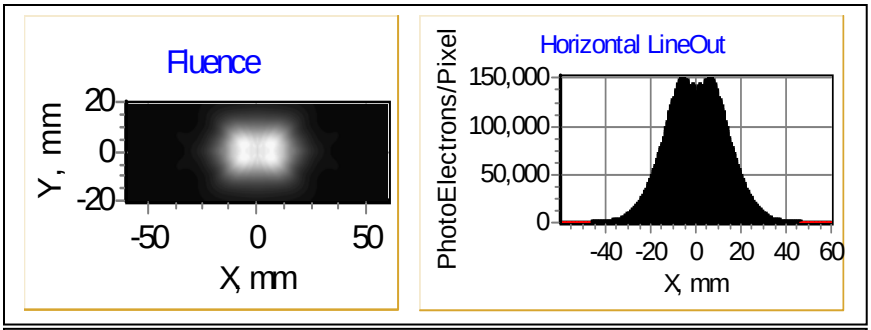

Figure 4: Simulated Direct Imager response to a single pulse of spontaneous radiation at 14.5 GeV in photoelectrons / pixel.

Figure 4 shows the calculated Direct Imager image, in photoelectrons per pixel, from exposure to one pulse of spontaneous radiation at the 14.5 GeV linac setting. The line out shows the photoelectron levels across the pixels in the central row. The image looks quite different than the raw image of spontaneous fluids at this point shown the preceding figure. The LSO has only absorbed spontaneous photons whose energies are < 40 keV while allowing higher energy photons to pass through. Note that the signal levels approach 150K electrons per pixel compared to a full well value of 327 K electrons. This is a good signal, about half scale on the CCD, and well above any noise sources.

To simulate the FEL embedded in the spontaneous background we add the FEL signal to the cube of spontaneous data. This is done by selecting the energy slice corresponding to the FEL energy and incrementing each spatial bin with the number of FEL photons that fall into its boundaries. Feeding this data, with the FEL at its saturated power level, into

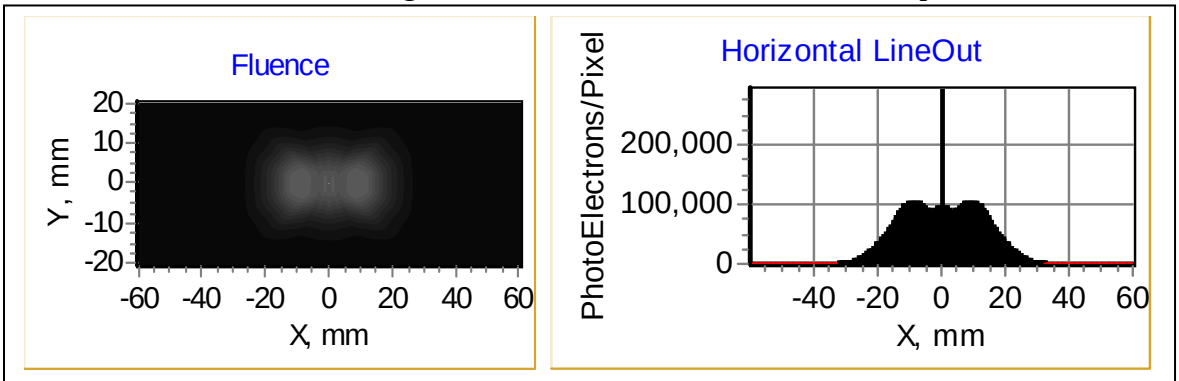

Figure 5: Simulated Direct Imager image of a single pulse of the combined FEL and spontaneous radiation at 14.5 GeV viewed through a 16.8 mm boron carbide attenuator. The FEL was assumed to be at its full-saturated power level.

the camera model results in an image whose central pixel is oversaturated by a factor of 10^4. Of course, the Direct Imager would not be put directly in the beam in this case because it would be damaged. Instead, we would run the 8 keV beam through 16.8 microns of boron carbide, which would attenuate the FEL by 10^{-4}, and then run the attenuated beam into the scintillator.

This situation has been simulated by taking the cube of FEL plus spontaneous data and calculating the number photons in each cell transmitted by the boron carbide creating

another cube representing the attenuated beam. Feeding the attenuated beam into the camera model results in figure 5, which shows what the Direct Imager would see after the boron carbide. The boron carbide hardly attenuates the spontaneous radiation, whose photoelectrons level is only slightly less than without it. The FEL shows up in the central pixel, which is nearly saturated, but not oversaturated.

Note that the FEL photoelectron levels in the camera are dependent on the spatial resolution of the scintillator/camera system at the scintillator. In figure 5, for technical reasons, we have assumed that this resolution was 300 x 100 μm, although the camera design can achieve resolutions much better than this.

How faint can the FEL be?

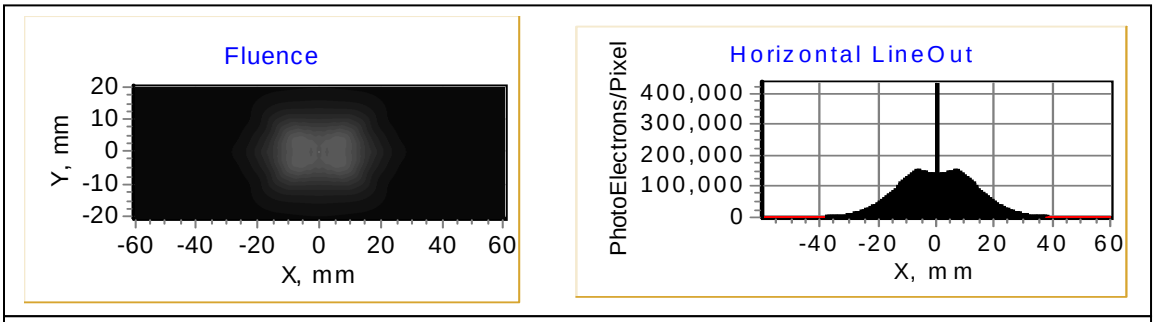

Figure 6: Simulated Direct Imager image of the spontaneous background plus a weak (0.01% of saturation) FEL at 14.5 GeV.

To simulate an underpowered FEL, as might be expected during commissioning, we created a data set consisting of the spontaneous data plus a small fraction of the FEL signal. Presumably in the case of a weak FEL we would put the Direct Imager directly in the beam since damage would not be an issue. Figure 6 shows the expected Direct Imager signal in response to the full spontaneous background plus an FEL (at 8.261 keV) reduced to 0.01 % of its saturated level. The FEL signal is clearly visible, in fact is slightly oversaturated, indicating that the FEL signal would still be visible even at power levels reduced from this. Again this calculation assumes a spatial resolution of 300 x 100 μm.

Beam simulations at 4.5 GeV

The situation is a little different when the linac is running at the 4.5 GeV setting. The total energy in the spontaneous background is lower but the 25 mm thick LSO absorbs nearly all of it. In fact the energy absorbed by the LSO is nearly the same in both the high energy and low energy case (1.205 mJ at 4.5 GeV and 1.576 mJ at 14.5 GeV) Figure 7 shows the response of the Direct Imager to the full spontaneous background at 4.5 GeV plus 0.01 % of the 826 eV FEL. Although the absorbed spontaneous power is nearly the saying it is spread out over a much larger area resulting in lower photoelectron levels. The reduced FEL signal is also clearly visible in the central pixels. Although the

signals are much lower than the signal at 14.5 GeV, they are still much larger than the noise levels.

Note that the spontaneous radiation signal will be at least 30 x lower when we are operating with all but the first undulator rolled away. This is probably at or below the current Direct Imager detection threshold at 4.5 GeV. To make sure that the LCLS detectors cover the range of fluxes expected, we must define the rollaway undulator

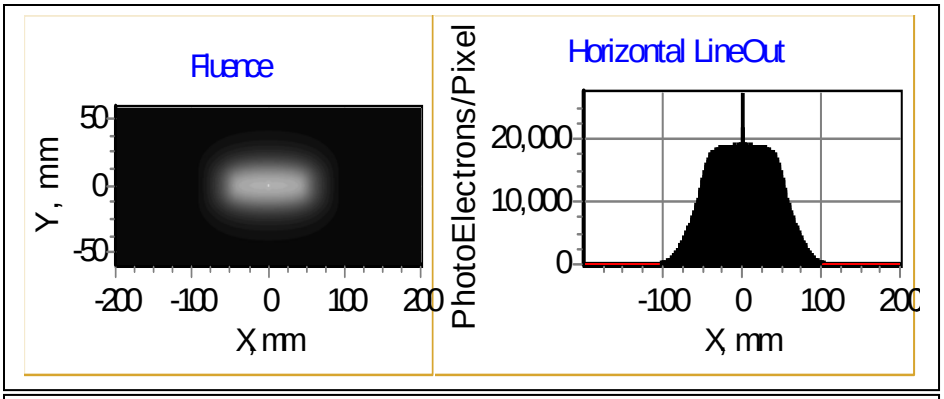

Figure 7: Simulated Direct Imager image of the spontaneous background plus a weak (0.01% of saturation) FEL at 4.5 GeV.

configurations that we will use during commissioning and generate corresponding near-field radiation patterns to feed into the detector simulations.

Commissioning with the Direct Imager

These results indicate that the Direct Imager will see the spontaneous background on a single shot over the range of linac settings from 4.5-14.5 GeV. The Direct Imager will need 10^{-4} attenuation for on-scale operation at full FEL power. The attenuation will not attenuate the spontaneous radiation so that the signal-to-noise will be smaller. Without attenuation, the Direct Imager will see the FEL at 0.01 % of its saturated power level at 4.5 GeV and significantly < 0.01 % at 14.5 GeV.

Reflections in the Undulator Vacuum Chamber

The undulator vacuum chamber is a long, thin, tube of copper that is highly polished on the inside. Because of the small radius of the tube, much of the spontaneous radiation strikes the inner surface at angles of incidence significantly below the critical angle (~22 mRad at 8.261 keV) and reflects back towards the center of the beam. We studied the resulting spatial distribution at the position of our diagnostics using a Monte Carlo simulation.

The Monte Carlo fires photons from a source distribution through materials and simulates the physics of the photoelectric effect, Compton scattering, and refraction and reflections at interfaces. To simulate the spontaneous radiation, we fed the Monte Carlo cumulative probability distributions for the energy spectra at each transverse position in the spontaneous radiation data as well as cumulative probability distributions for the transverse spatial coordinate of the photons. The Monte Carlo uses these distributions to generate the final photon position and the photons energy. The initial photon position is randomly selected from the electron distribution along the length of the undulator, and the photon's direction is set along the vector from the initial to the final position. The Monte Carlo starts the photons at their initial positions and tracks them through any material objects along their path. In the absence of any material objects, the final photon spatial/energy distributions match the UCLA calculations at the position of the UCLA calculation.

For simulations of the undulator vacuum chamber, we add a 130 m long hollow cylinder of copper with inner diameter of 5 mm, outer diameter of 6 mm, and a perfectly smooth inner surface. The photons hitting the inner cylinder are reflected or transmitted according to Snell's law, and further tracked downstream.

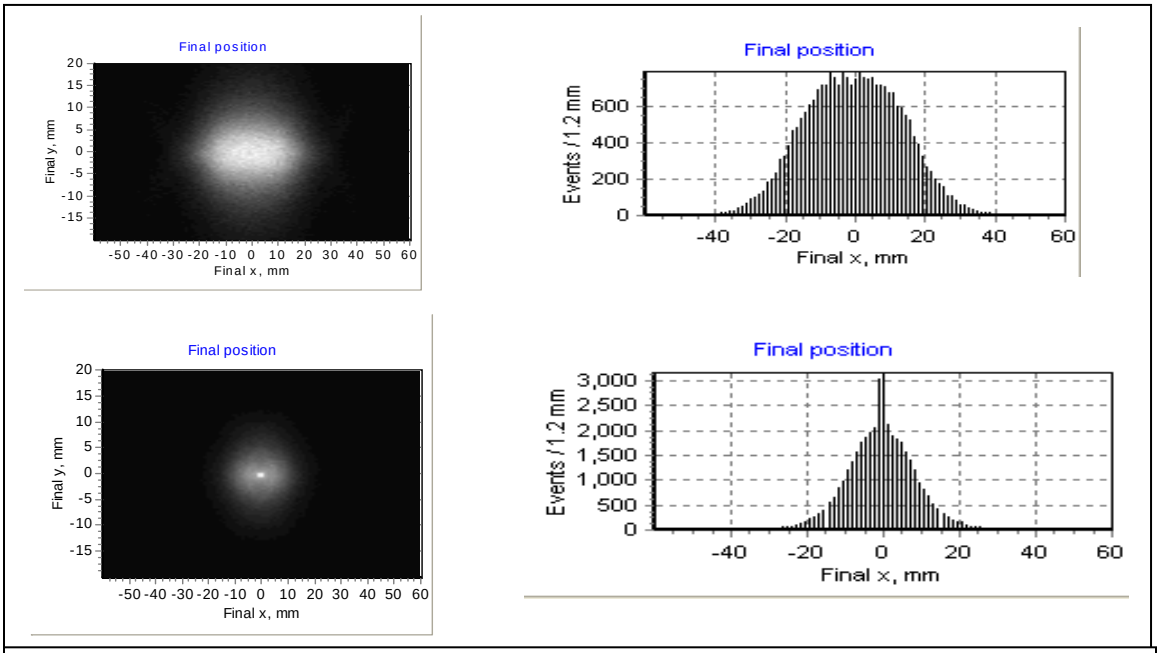

Figure 8: Monte-Carlo simulations of the 14.5 GeV spontaneous radiation pattern at the entrance to the near hall without an undulator vaccum pipe, top, and with an undulator vaccum pipe, bottom. Almost all photons that strike the pipe reflect, resulting in a narrow, more focused spatial distribution.

Figure 8 shows simulated photon distributions at the position of the Direct Imager in the first hutch of the NEH with and without the copper tube at 14.5 GeV. The top plot in figure 8 shows the distributions without the tube and has the same spatial/energy distributions as the UCLA calculation in figure 3. (Note that the units in the distributions

of figure 8 are total photons/bin whereas the units in the distributions shown in figure 3 are total energy/bin.) The horizontal line out shows a FWHM of 40 mm and a peak of ~700 photons/bin (out of 1 M generated.) The bottom distributions show the situation with the vacuum pipe in place. Because the angles are well below the critical angle, all photons that struck the smooth cylinder in the simulation are reflected without absorption, and some of them are reflected multiple times without absorption. The resulting distribution at the Direct Imager looks narrower and more focused with a bright spot in the middle. The horizontal line out shows a FWHM of 20 mm and a peak of 3000 photon/bin, out of 1 M generated, an increase in spontaneous background of a factor of 4.3.

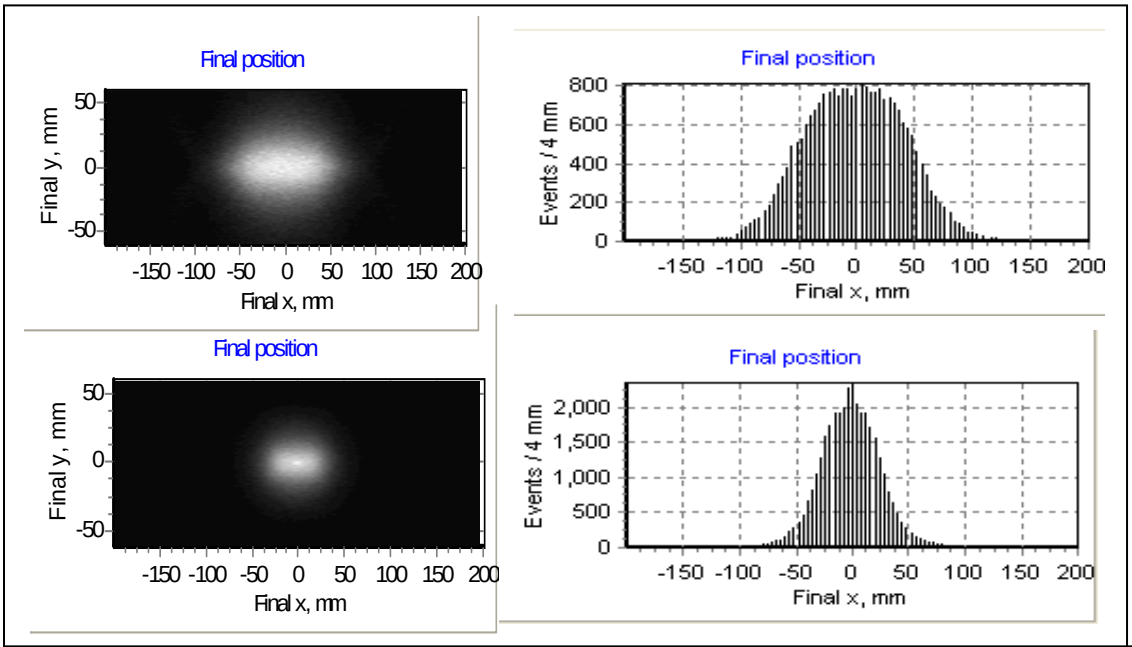

Figure 9: Monte-Carlo simulations of the 4.5 GeV spontaneous radiation pattern at the entrance to the near hall without an undulator vaccum pipe, top, and with an undulator vaccum pipe, bottom. The spatial distribution, with the undulator pipe in place, has a FWHM of 50 mm.

Figure 9 shows the simulated photon distributions at the position of the Direct Imager in the first hutch of the NEH with and without the copper tube at 4.5 GeV. Without the tube the distribution has a FWHM of 100 mm, which narrows down to 50 mm with the tube. The presence of the tube increases the number of spontaneous photons in the center by the ratio of 3000/800 = 3.75.

We have also run simulations were the tube is tilted with respect to the electron beam. We observe that small tilt angles, of the order of 20 μRad, significantly change the appearance of the spatial distributions at the position of the Direct Imager.

We conclude from the studies of vacuum chamber reflections that 1) we will see a lot of reflections of the spontaneous radiation off of the vacuum tube; 2) the reflections will

increase the spontaneous background in the center by factors of three or four; and 3) twists and tilts in the vacuum chamber will make it hard to interpret the observed spontaneous radiation pattern.

Apertures

All distributions presented above are calculated under the assumption that there are no additional apertures restricting the spray of spontaneous radiation (except for the case of the undulator vacuum tube discussed above.) In reality, the radiation pattern visible at the entrance of the NEH will be restricted by the diameter of the vacuum pipes and the apertures required for radiation safety. An *upper bound* on the diameter of the transport system up to the entrance of the NEH might be taken from the spatial distribution at 4.5 GeV (which has the largest divergence) after reflection off of the tube (since we will certainly have the tube.) This is the distribution in the bottom of figure 9. Transporting twice the FWHM in this case would require an aperture of 100 mm at the entrance to the NEH and proportionately smaller apertures at positions closer to the end of the undulator. The aperture upper limits calculated this way raise safety and cost concerns since they are roughly 10 times larger than aperture diameters commonly used for radiation protection in electron beam and dump areas.

Observing out to the edges of the spontaneous radiation pattern is not a current requirement. We do not foresee any quantitative diagnostic procedure defined for commissioning that requires a measurement of the full spontaneous radiation pattern. Furthermore, we don't even want to transport the full spontaneous radiation pattern to the users, but plan to place three fix masks in the FEE to restrict the beam extent to a small region surrounding the FEL.

The aperture sizes will therefore be set by safety and cost considerations and can be smaller than the upper limit suggested above. Nevertheless, in the interests of maximum flexibility during commissioning, we are assessing aperture schemes that allow the full spontaneous distribution to be transported into the FEE for observation during commission, while protecting personnel with a tight aperture just in front of the entrance to the NEH. In any case the final sizes of the apertures need to be specified and incorporated into the detector simulations.

Future work

Our goal for the next six months is to use our simulations to determine engineering specifications for the diagnostic instrumentation. We are currently in the process of optimizing the choice of scintillators, microscope objectives, and CCD selections for the Direct Imager. Next, we will develop specifications for the gas and solid attenuators after modeling Direct Imager response through the attenuators systems. Then, we will specify and model the Indirect Imager mirror system and its energy dependent response to the FEL plus spontaneous background. Independent of the detector modeling, we must

update our beam models to take into account the effects of reflections in the undulator vacuum tube as well as the radiation safety apertures once finalized.

We also need to study the detector response to the FEL gain vs. Z measurement in the rollaway undulator scenario. This would require 1) calculating the near field radiation pattern as individual undulators are added to the beam line; 2) simulating the FEL for each of these undulator configurations, which is difficult because of the statistical effects that are dominant for small numbers of undulators; and 3) combining the spontaneous and FEL data and feeding it into the camera models.

XTOD Commissioning Summary

In summary, the Title I process has set the conventional layout geometry, and the new positions for the attenuators, further from the end of the undulator, significantly reduce requirements, making the attenuator designs more robust. We now have beam-modeling codes in place that interface to our diagnostic simulations and can create simulated images of detector response to the FEL and spontaneous backgrounds. We are predicting that reflections off the undulator vacuum chamber will seriously distort the spontaneous radiation pattern. We are currently working on a detailed model of our Direct Imager camera in order to specify its scintillator and attenuator thicknesses and CCD parameters. Similar models will be constructed to generate specifications for the Indirect Imager and the other diagnostics.